NASA DEVELOP National Program
North Carolina – NCEI

Summer 2024

Asheville Urban Development II

Mapping Urban Heat to Support Cooling Initiatives and Climate Resilience Planning in the Greater Asheville Area

DEVELOP Technical Report

August 9th, 2024

Kimberly S. Becerril (Project Lead)
Caleb V. Kluchman
Sarah L. McMullen
Caroline M. Tintinger

Advisors:
Douglas Rao, NOAA National Centers for Environmental Information, North Carolina Institute for Climate Studies (Science Advisor)
Edward Macie, Board of Directors, Asheville GreenWorks, CoA Urban Forestry Commission (Science Advisor)
Molly Woloszyn, NOAA National Integrated Drought Information System (Science Advisor)

Previous Contributors:
Darcy Gray (Project Lead)
Amiya Kalra
Amy Kennedy

Lead:
Tallis Monteiro (North Carolina – NCEI)

1. Abstract

Asheville, North Carolina experiences the urban heat island effect, where temperatures in the city are higher than in surrounding rural areas. This effect intensifies with increased urbanization and less vegetative cover. Asheville's urban heat island was exacerbated by population increases and tree cover decline, escalating the need for heat mitigation. We partnered with the City of Asheville's Sustainability Department and Asheville GreenWorks whose actions prioritize sustainable city planning and equitable climate resilience. Using NASA Earth observations and ancillary datasets we spatially mapped urban heat, heat vulnerability, and cooling and adaptive capacity from 2019-2023. To map urban heat, we used Landsat 8 and 9 Operational Land Imager and Thermal Infrared Sensor for land surface temperature and albedo data and the ECOsystem Spaceborne Thermal Radiometer Experiment on Space Station for evapotranspiration data. We assessed heat vulnerability using the urban heat data and the Centers for Disease Control and Prevention's Social Vulnerability Index. To evaluate cooling and adaptive capacity we used the InVEST Urban Cooling Model, integrating our heat vulnerability analysis with land use and cover data from Sentinel-1 Synthetic Aperture Radar and Sentinel-2 Multispectral Instrument. Our results revealed distinct spatial patterns of urban heat, heat vulnerability, and cooling and adaptive capacity in Asheville with downtown as the focal hotspot and an outward decreasing radial pattern. These findings highlight targeted need for interventions to reduce heat impacts, address environmental injustices, and enhance climate resilience. Our project provided research to local organizations that can be used for heat mitigation in the greater Asheville area.

Key Terms

albedo, Earth observations, evapotranspiration, heat mitigation, heat vulnerability, land surface temperature (LST), urban heat island (UHI)

2. Introduction

2.1 Background Information

Urban heat islands (UHIs) are urbanized areas that experience higher temperatures than adjacent rural areas (Environmental Protection Agency, n.d.). Variation between urban and rural land surface temperatures (LST) is caused by three factors: minimal vegetation, anthropogenic activities, and urban design (Nuruzzaman, 2015; Stache et al., 2022). Evapotranspiration from vegetation and soil reduces temperatures; therefore, temperatures rise in cities with inadequate vegetation (Qiu et al., 2013). Heat increases in urban areas due to anthropogenic activities including transport, industry, and air conditioning (Tong et al., 2021). City design augments heat by blocking wind flow and trapping reemitted insolation (Phelan et al., 2015). These factors create UHIs that experience 0.5°C to 4°C higher daytime temperatures compared to surrounding rural areas (EPA, n.d.).

UHIs result in copious environmental, health, and economic consequences. Environmentally, temperatures rise, water quality and quantity decline, and air pollution increases (Phelan et al., 2015), threatening human health by escalating heat stress, heat-related illnesses, and morbidity (Tong et al., 2021). Although these adverse effects occur ubiquitously across UHIs, severity is uneven. Hotspots are areas where severe LST is compounded by low albedo and the lack of evapotranspiration (Tong et al., 2021).

Socially vulnerable populations are significantly more likely to live in hotspots; these are heat-vulnerable communities (Mitchell & Chakraborty, 2015; Tong et al., 2021). Historical discriminatory government and urban planning practices, including redlining, led to the spatial correlation between social vulnerability and heat resulting in neighborhoods lacking vegetation or heat-resistant infrastructure (Swope et al., 2022). In UHI hot spots, heat-vulnerable communities have high heat exposure, limited capacity to adapt to high temperatures, and notable heat-related health risks caused by socioeconomic and demographic factors (Reid et al., 2009; Bao et al., 2015; Shahmohamadia et al., 2015).

2.2 Study Area and Period

Located in western North Carolina, Asheville has an area of 117.2 km (*Figure 1*) and a population of 95,056 as of 2023 (U.S. Census Bureau, n.d.). Asheville's population has increased over 40% in the last 35 years and tree cover has declined by an estimated 6.4% since 2008, indicating a loss in Asheville's cooling ability (U.S. Census Bureau, n.d.; The City of Asheville, 2019). Increased population, reduced tree cover, infrastructure expansion, and rising temperatures have increased stress on vulnerable communities, making Asheville an apt study area.

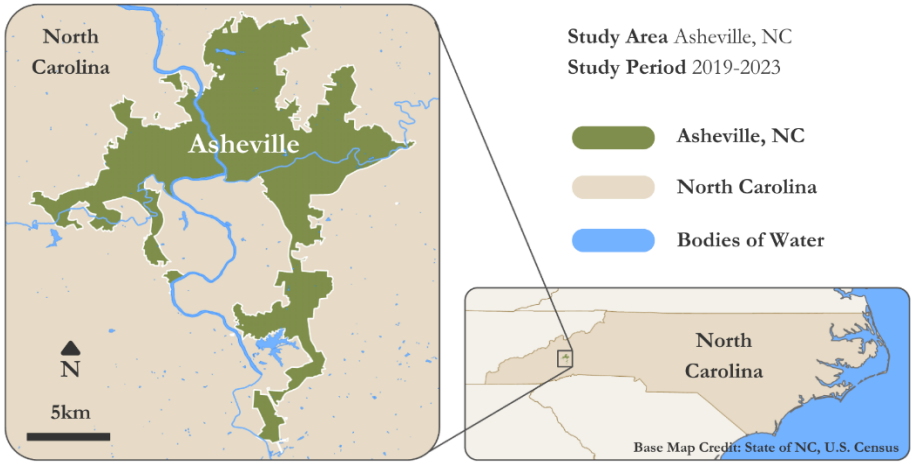

Figure 1. Map of Asheville, North Carolina

2.3 Project Partners & Objectives

We partnered with Asheville GreenWorks (GreenWorks) and the City of Asheville (CoA) Sustainability Department to carry out the project. GreenWorks is committed to building equitable climate resiliency in Asheville through planting trees and other initiatives (Asheville GreenWorks, 2022). On July 24, 2023, the projected hottest day of 2023, GreenWorks mapped the UHI effect across Buncombe County, NC neighborhoods supported by National Oceanic and Atmospheric Administration (NOAA) to identify neighborhoods most in need of tree planting.

The City of Asheville (CoA) is committed to implementing sustainable practices and city design, focusing on supporting vulnerable communities (The City of Asheville, 2020). To go about this, the CoA instigated its Climate Justice Initiative (The City of Asheville, n.d.). As part of this initiative, the CoA collaborated with Black, Indigenous, and People of Color (BIPOC) community leaders created the Climate Justice Index and the Asheville Climate Justice Map (The City of Asheville, n.d.-a), which includes data collected by the 2019 NASA DEVELOP Asheville Urban Development I team (AUD1). The CoA is also building an Urban Forest Master Plan, including heat mitigation strategies for climate resilience, such as strategic tree planting (The City of Asheville Urban Forestry Commission, 2023).

The AUD1 project mapped Asheville's LST change between 1984 and 2018, tree cover, and two socioeconomic factors influencing social vulnerability (Gray et al., 2019). We expanded upon the AUD1 project, mapping urban heat to support cooling initiatives in Asheville from 2019 to 2023. Our objectives were to investigate the impacts of UHIs based on environmental and social vulnerability data. We determined the feasibility of using remote sensing to identify areas for potential heat mitigation. We produced an urban heat map to analyze hot spots utilizing LST, evapotranspiration, and albedo data from Earth observations. Since the AUD1 team mapped tree cover, we used evapotranspiration to indirectly indicate vegetation, expanding the research scope (Moss et al., 2019). We also evaluated the spatial correlation between hot spots and social vulnerability by combining the Centers for Disease Control and Prevention (CDC) social vulnerability index (SVI) with the urban heat map, creating a heat vulnerability map (Center for Disease

Control, n.d.). Finally, we applied the InVEST Urban City Cooling Model to the heat vulnerability map to produce a UHI mitigation and adaptation measures map (Stanford University, n.d.). These maps informed the heat mitigation efforts of the CoA and GreenWorks. Potential heat mitigation efforts include tree planting and alternative cooling methods such as cooling pavements and green and white roofs (Phelan et al., 2015; Knight et al 2021). The heat vulnerability map amended the Asheville Climate Justice Index and updated the Asheville Climate Justice Map with the most current data, up to 2023.

3. Methodology

3.1 Data Acquisition

Table 1

Satellite Platforms and Sensors Used for Data Acquisition and their Parameters and Use

Platform and Sensors	**Parameter(s)**	**Use**
Landsat 8 *Operational Land Imager (OLI) and Thermal Infrared Sensor (TIRS)*	Land Surface Temperature and Albedo	We used Landsat 8 imagery to measure LST and albedo for the warm months (May 1st to September 30th) over the study period 2019-2023.
Landsat 9 *Operational Land Imager 2 (OLI-2) and Thermal Infrared Sensor 2 (TIRS-2)*	Land Surface Temperature and Albedo	We used Landsat 9 imagery to measure LST and albedo for the warm months (May 1st to September 30th) of 2022 and 2023.
ISS *ECOsystem Spaceborne Thermal Radiometer Experiment on Space Station (ECOSTRESS)*	Evapotranspiration	Level 3 data was used to create a median composite of evapotranspiration for the warm months (May 1st to September 30th) from 2019 to 2022.
Sentinel-1 *Synthetic Aperture Radar at C-band frequencies (C-SAR)*	Land Use Land Cover	We used Sentinel-1 data through the ESA WorldCover Land Use Land Cover 2021 product.
Sentinel-2 *Multispectral Instrument (MSI)*	Land Use Land Cover	We used Sentinel-2 data through the ESA WorldCover Land Use Land Cover 2021 product.

3.1.1 Land Surface Temperature and Albedo Data Sources

Our team acquired Landsat 8 (Level 2, Collection 2, Tier 1) and Landsat 9 (Level 2, Collection 2, Tier 1) data to calculate land surface temperature and albedo data in Google Earth Engine (GEE) (U.S. Geological Survey, 2020). Landsat 8 and 9 satellites carry the Operational Land Imager (OLI and OLI-2, respectively) and Thermal Infrared Sensor (TIRS and TIRS-2, respectively) instruments. We utilized Landsat 8 imagery to measure LST and albedo over the study period 2019- 2023, incorporating Landsat 9 for 2022 and 2023, to include data following its deployment in 2021. For optimal analysis of the Asheville UHI, our team filtered both collections to include data for only the warm months: May 1st to September 30th. Both Landsat 8 and 9 have a grid spacing of 30x30m, making them suitable sources for detailed LST and albedo data (Table 1). It is important to note that the intrinsic spatial resolution of TIRS and TIRS-2 sensors is only 100x100m. The TIRS and TIRS-2 products are actually "oversampled" and gridded at 30x30m to make them easily compatible with OLI and OLI-2 observations.

3.1.2 Evapotranspiration Data Sources

Our team retrieved ECOSTRESS (Hook & Fisher, 2019) evapotranspiration data (PT-JPL Daily L3 Global 70m) from the Land Processes Distributed Active Archive Center through the Application for Extracting and Exploring Analysis Ready Samples (AppEEARS) (AppEEARS Team, 2024). ECOSTRESS is equipped with

the Prototype Hyperspectral Infrared Imager Thermal Infrared Radiometer (PHyTIR) sensor. The level three data was available up to February of 2023, so a median composite was created for the warm months from 2019 to 2022. Analyzing Asheville's spatial (rather than temporal) evapotranspiration trends was a project goal, therefore missing 2023 data was not a hindrance (Table 1).

3.1.3 Social Vulnerability Data Source

We obtained data on social vulnerability through the CDC and the Agency for Toxic Substances and Disease Registry (ATSDR) SVI, utilizing the latest available U.S. Census Bureau data from 2022 (Center for Disease Control and Prevention, n.d.). We used the CDC/ASTDR SVI because the CoA used this index in the existing Climate Justice Map, and it is a standard national measure of social vulnerability. The SVI includes four main themes: socioeconomic status, household characteristics, racial and ethnic minority status, and housing type and transportation (Center for Disease Control and Prevention, n.d.). Each component encompasses variables to comprehensively delineate populations' vulnerable demographic composition, measured as a percentage, at the census tract scale (Center for Disease Control and Prevention, n.d.). First, socioeconomic status encompasses demographic data on the percentage of individuals below 150% poverty, unemployed, burdened with housing costs, with no high school diploma, and/or no health insurance. Second, household characteristics include those aged 65 and older, aged 17 & younger, a civilian with a disability, single-parent households, and/or with English language proficiency. Third, racial and ethnic minority status encompasses individuals who are Hispanic or Latino (of any race), Black and African American, American Indian & Alaska Native, Asian, Native Hawaiian and other Pacific Islander, two or more races, and/or other races. The fourth component, housing type and transportation encompasses the percentage of the population residing in multi-unit structures, mobile homes, in crowding, with no vehicle, and/or living in group quarters.

3.1.4 Land Use and Cover Data Sources

We obtained land use and cover (LULC) data from the European Space Agency (ESA) WorldCover project, containing modified Copernicus Sentinel-1 and Sentinel-2 data (from the year 2021) processed by the ESA WorldCover consortium (Zanaga, et al., 2021). The LULC data was at 10x10m resolution and included six land cover classes for our defined study area: tree cover, grassland, cropland, built-up, sparse vegetation, and permanent water bodies (ordered from most to least prevalent). The canopy cover data was provided by the City of Asheville's Sustainability Department (City of Asheville, 2018). The canopy cover data was for the years 2008- 2018 (Table 1).

3.2 Data Processing

3.2.1 Land Surface Temperature Data Processing

We processed the LST data, utilizing the UHEAT Urban Development PUP Spring 2022 team's Land Surface Temperature Heat Script from the Urban Heat Island Toolkit in the NASA DEVELOP Google Earth Engine 5.3.3 (GEE) repository as a template (Agrawal, et al., 2022). First, as per the script, the parameter limits for temperature were set from 10-40°C, which edited the LST data display. This range was chosen because median summer temperatures in Western NC do not fall below 10°C or rise above 40°C. We used median instead of maximum values to more accurately represent the typical condition of warm month temperatures. Median values are also less susceptible to the impact of outliers than mean values. Second, we spatially defined the study area by setting the coordinates and geometry for Asheville, NC (35.3951493 - 35.6786576°N, 82.4262664 - 82.6766268°W). Calling eight image collections, six from Landsat 8 covering 2019-2023 and two from Landsat 9 for 2022 and 2023, established the Landsat surface temperature collection. These eight image collections were merged into one layer. We then used image pre-processing functions to convert the data from Kelvin to Celsius, applied a mask to remove cloudy pixels, and applied the mosaic-by-date function. The mosaic function created a single image from the image series captured over the defined period from 2019-2023. Adding a temperature palette allowed for LST visualization. Then, the date mosaic was set to visualize pixels representing the median LST value for each 30x30m area. The result was a visualization in GEE of the greater Asheville area showing median LST from 2019 to 2023 using graduated color symbology. The LST code visualization was exported into Google Drive as a TIFF file.

From the TIFF file, raster band ST_B10, was uploaded into ArcGIS Pro 3.1.2 for further processing. The following tools were used to create an attribute table and, ultimately, a vector from the raster. The raster's float numbers were converted to integers as a preliminary step to create an attribute table. To do this, we used the Raster Calculator tool to multiply the raster by 100,000 and applied the Int tool to convert the raster data into integers. For reference, the Int tool drops the numbers after the decimal point so multiplying those values by 100,000 helps maintain their precision. Then, to create the new attribute table, we used the Build Raster Attribute Table tool. At this point, the raster could be converted to a vector. We used the Raster to Polygon tool, without selecting the Simplify Polygons setting, to convert the raster dataset into a vector or polygon dataset. Using a vector dataset allows for easier data analysis with other vector datasets such as data from the U.S. Census. After creating the LST vector dataset, the values that were converted to integers were reconverted to floats by transcribing them into a new field with a double type, or float type, naming it Celsius, and dividing it by 100,000. Finally, we employed the Spatial Join tool between the LST vector dataset, and the census block groups to calculate the mean LST value per Census Block Group. The result was a choropleth map of Asheville displaying census block groups' mean LST value for 2019- 2023.

3.2.2 Albedo Data Processing

Utilizing the GEE script from 3.2.1 as a template, we modified the script to process albedo data, rather than LST. As done to process the LST data, we defined our study area as Asheville, NC and called in 8 image collection datasets from Landsat 8 and 9. We then calculated albedo using OLI bands 1 (Coastal/Aerosol), 3 (Green), 4 (Red), 5 (Near Infrared), and 7 (Short Wave Infrared (SWIR) – 2) with the following equation (Equation 1; Yale University, n.d.). Each variable represents the associated band. For example, 0.130 x b3 means 0.130 times the value of band 3 for that pixel.

$$Albedo = \frac{0.356 * b1 + 0.130 * b2 + 0.073 * b4 + 0.085 * b5 + 0.072 * b7 - 0.0018}{0.356 + 0.130 + 0.373 + 0.085 + 0.072} \quad (1)$$

We used the merge function to aggregate the albedo data image collections into one layer. Using the mosaic by date function, we generated a list of unique dates and merged and separated each unique date into image sets. We removed all unrelated bands from the image to reduce processing time. The albedo code visualization was exported into Google Drive as a TIFF file.

The TIFF file was imported into ArcGIS Pro 3.1.2 for further processing. We used the Raster Calculator tool to convert the data into integers with minimal decimals. Using the Int tool, we truncated the integers, to exclude negligible data. Next, we used the Raster to Polygon tool, without selecting the Simplify Polygons setting, to convert the raster dataset into a vector or polygon dataset. We then spatially joined the spatial census block data, using mean as the merge rule for the relevant values. The result was a choropleth map of Asheville displaying the albedo values of each census block group for 2019 – 2023.

3.2.3 Evapotranspiration Data Processing

ECOSTRESS level 3 data lacks geographic data in its raw h5 file form, so to use it, we either had to run a swath to grid Python script, provided by the LP DAAC Data User Resources, or make an 'Extract Area Sample' request through AppEEARS (AppEEARS Team, 2024). Both options were tested and evaluated, and we found that AppEEARS was the more efficient and error-proof process. We uploaded the study area vector file for the data request, entered the date range of May 1st to September 30th, and selected the "Is Date Recurring" box and entered the year range of 2019- 2022. We selected the ECO3ETPTJPL 001, 70m, ISS-dependent, (2018-07-09 to Present) product, and the EVAPOTRANSPIRATION_PT_JPL_ETdaily layer.

Once the data was sent from AppEEARS, all the layers were imported into ArcGIS Pro. We combined all the Daily ET raster layers into one raster using the Mosaic to New Raster tool. We used the mean operator since the median was not available. The mosaic was then turned into a polygon using the raster to polygon tool to ensure the polygons were not simplified and then clipped to our study area. Next, we spatially joined the

polygons to the census block spatial data, using mean as the merge rule for the relevant values. The result was a choropleth map of Asheville displaying census block groups' evapotranspiration values for 2019 - 2022.

3.2.4 Social Vulnerability Data Processing

The social vulnerability data from the U.S. Census American Community Survey (ACS) was processed at the census tract scale by the CDC/ATSDR to create the SVI (Center for Disease Control and Prevention, n.d.). To do this, the CDC processed and summed each of the four themes to calculate their overall percentile rankings per census tract (Center for Disease Control and Prevention, n.d.). The themes' values were then summed and classified using a scale ranging from zero to one to create an SVI ranking ("RPL_THEMES") for each census tract (Center for Disease Control and Prevention, n.d.). We isolated the final census tract SVI ranking ("RPL_THEMES") from the CDC/ASTDR SVI CSV file. Then, to spatially rescale the data to be analogous with the other data sets (LST, albedo, and evapotranspiration), all census blocks within a census tract were assigned the tract-level SVI value.

The processed census block SVI data was uploaded into ArcGIS Pro. We used the Spatial Join tool to join the census block groups to the SVI data. The join operation was one-to-one, so all target features were kept, with the intersect match option, and a mean merge rule. This step transcribed the CDC SVI data into the Asheville census block groups. The result was a choropleth map of Asheville displaying SVI at the census block scale.

3.2.5 Heat Vulnerability Data Processing

We used the min-max normalization method to process the datasets to create the urban heat and heat vulnerability indices. In this standardization method, the minimum value transforms to zero, and the maximum value transforms to one. All other values transform into a decimal between zero and one (the minimum and maximum values). This process is delineated in the min-max normalization equation (Equation 2):

$$\frac{value - min}{max - min} \tag{2}$$

To create the urban heat index, we first processed the raw raster data by calculating the mean value for the pixels within each census block group vector for LST, albedo, and evapotranspiration. Then, we standardized the LST, albedo, and evapotranspiration datasets using the min-max normalization formula (Equation 2). We weighed the data, to emphasize the impact of LST (heat exposure). Adaptive capacity is measured by albedo and evapotranspiration, which are indirect effectuating factors of urban heat. Therefore, these factors have less influence on hot spot formation than LST. To accurately represent the relative influences of urban heat, we used the following equation adapted from Weber et al. (2015) and the AUD1 team (Equation 3) to weigh the data. In the urban heat equation, heat exposure was measured by LST, and adaptive capacity was measured by adding albedo and evapotranspiration.

$$urban\,heat = heat\,exposure \cdot (1 - adaptive\,capacity) \tag{3}$$

With the standardized, weighted urban heat values at the census block group level, we created the urban heat map. We then imported the data into ArcGIS Pro. We processed it using the same methodology for the LST, albedo, and evapotranspiration datasets but tailored some processing steps for the urban heat index specifications. The result was an urban heat map for Asheville, NC with data from 2019 – 2023.

To create the heat vulnerability index, we combined the urban heat and SVI indices. In accordance with the weighting of the urban heat equation (Equation 3), adaptive capacity was given less weight. This process is delineated in the following equation (Equation 4). In the heat vulnerability equation, heat exposure was

measured by LST, social vulnerability was measured by the SVI, and adaptive capacity was measured by albedo and evapotranspiration.

$$heat\ vulnerability\ =\ heat\ exposure\ \cdot\ social\ vulnerability\ \cdot\ (1-adaptive\ capacity) \tag{4}$$

With the heat vulnerability scores for Asheville's census block groups, we created the heat vulnerability map. We imported the heat vulnerability index data into ArcGIS Pro and processed it using the same data processing methodology for the urban heat map. The result was a heat vulnerability map for Asheville, NC for data from 2019 - 2023. This map combined the variables of heat exposure (LST), social vulnerability (demographic and socioeconomic composition of communities), and adaptive capacity (albedo and evapotranspiration).

3.3 Data Analysis

To evaluate the cooling and adaptive capacity of the CoA, we used the InVEST Urban Cooling Model (Stanford University, n.d.). To get an output from the model of cooling capacity, we input our study area shapefile, our user-made biophysical characteristics CSV file, and evapotranspiration, albedo, and LULC raster datasets from ESA WorldCover and the CoA. As per the model's requirement to use a spatial projection with linear units, we used the WGS 84 Web Mercator.

The user-made biophysical characteristics table had four required columns, which were used to identify the land use code ("lucode"), designate which land uses are green areas ("green_area"), designate average albedo for that land use ("albedo"), and designate average canopy cover for that land use ("shade"). The final column ("kc"), used to measure expected evapotranspiration for each land use, was edited to convert all values to one because we had high-resolution evapotranspiration. We qualitatively assessed land cover classes to determine whether they were primarily vegetation or could contain vegetation. LULC classes of Tree Cover, Grassland, Copland, and Sparse Vegetation were assigned as green areas, while Built-up and Permanent Water Bodies were not. Albedo was calculated using Zonal Statistics as a Table tool in ArcGIS Pro, and the average albedo value for each land cover class was recorded. Average shade was calculated using the Summarize Within tool using ArcGIS Pro, and the average shade value for each land cover class was recorded.

The InVEST model processed the data using the following equation (Equation 5; Stanford University, n.d.). The result was a raster, with values ranging from zero to one. Low values represent low cooling capacity, or the lack of cooling measures, meaning low albedo, low evapotranspiration, and low canopy cover or shade. High values represent high cooling capacity.

$$CC_i\ =\ 0.6\ \cdot\ shade\ +\ 0.2\ \cdot\ albedo\ +\ 0.2\ \cdot\ ETI \tag{5}$$

To create our adaptive capacity map, we input the heat vulnerability index into the InVEST model with the cooling capacity data. We did this by running an Attribute Join in ArcGIS Pro between the two layers, and then selecting bivariate colors in symbology. A custom pallet was made for the four-by-four legend, with extremes taken from the associated layer pallets. The result was a bivariate map combining the heat vulnerability index and the InVEST cooling capacity output.

4. Results & Discussion

4.1 Analysis of Results

4.1.1 Urban Heat Island Hot Spot Analysis

The urban heat map (Figure 2) displays heat exposure in the CoA and the three contributing factors: LST (Figure 2A), albedo (Figure 2B), and evapotranspiration (Figure 2C). LST was highest in downtown Asheville and decreased radially outward from the city center (Figure 2A). However, West and South Asheville were inconsistent with this pattern, having moderately high LST which we attribute to the higher population densities and urban build-up in these areas. Northeast Asheville had the lowest LST, due to greater vegetation cover in this area (Figure 2A; Gray et al., 2019). Albedo was highest in the city center in downtown Asheville (Figure 2B). This was followed by South Asheville in Arden and at the Asheville Regional Airport (Figures 2B and A1). The remainder of the city had low albedo, with the peripheral areas having the lowest albedo (Figure 2B). This is consistent with the amount of vegetative cover, as vegetation can have low albedo rates (Gray et al., 2019). Albedo is a complex variable that does not always correlate with urban heat. Evapotranspiration was highest in the census block groups near or adjacent to the edge of the CoA's boundaries and lowest in the inner city (Figure 2C). Arden and the airport area were incongruent with this pattern, having moderate evapotranspiration levels, due to urban buildup and lack of vegetation in these areas (Gray et al., 2019). The city center in and around downtown Asheville had the lowest evapotranspiration levels, consistent with the dense urban landscape. The radial pattern of evapotranspiration demonstrates the correlation between evapotranspiration and vegetation: the more vegetation, the more evapotranspiration, and vice versa.

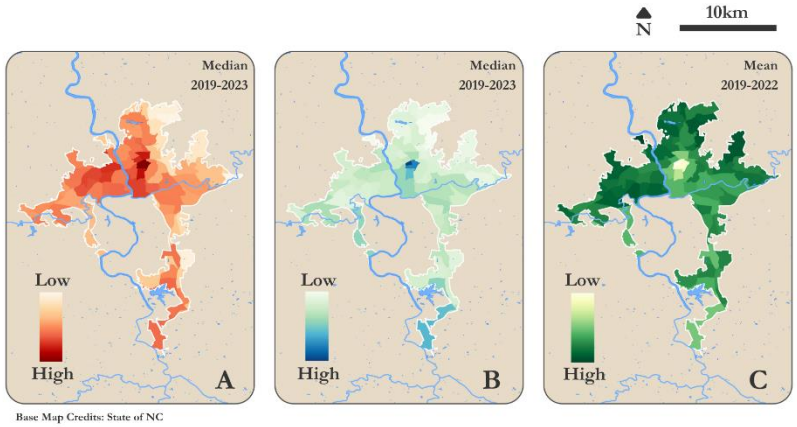

Figure 2. Land Surface Temperature (A), Albedo (B), and Evapotranspiration (C) Maps of Asheville, NC

The data shows that there is a distinct relationship between these three variables. Generally, where there was low LST, albedo was also low, and evapotranspiration was high. Vegetation typically has a relatively low albedo and results in high evapotranspiration, indicating the important role vegetation plays in reducing LST. This cooling effect is evident in the periphery of each map (*Figures 2A, B and C*), where a greater proportion of the land cover is more densely vegetated with trees (Gray et al., 2019). Alternatively, in the city center, where unnatural landcovers dominate the landscape and tree cover is sparse, LST is high, albedo is moderate, and evapotranspiration is low.

These three map layers were combined to create the urban heat map (*Figure 3*). The urban heat map shows that the city center was the CoA's most severe hot spot, closely followed by the areas directly surrounding downtown, and the area south of Shiloh and north of Arden (*Figures 3 and A1*). Overall, urban heat manifested in a pattern whereby urban heat decreased with distance from the city center (*Figure 3).* Areas with the highest urban heat had high LST compounded by low albedo and low evapotranspiration, and vice versa (*Figure 3*). The area south of Shiloh and to the north of Arden was an exception to this spatial pattern, with relatively high urban heat levels despite its distance from the city center, however, this is consistent with the level of urban buildup in this area (*Figures 3 and A1*).

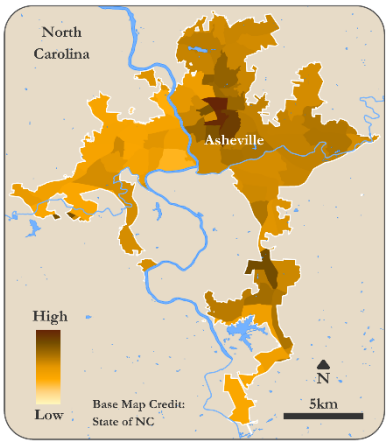

Figure 3. Urban Heat Map of Asheville, NC

4.1.2 Social Vulnerability Analysis

The social vulnerability map (Figure 4) shows the relative vulnerability of Asheville communities based on the CDC/ASTDR SVI. The most socially vulnerable neighborhoods were downtown, Emma, and in South Asheville to the east of Shiloh and in Biltmore Park (Figures 4 and A1). Broadly, the communities of West and South Asheville were moderately vulnerable (Figures 4). The stretch of West Asheville extending south towards Bent Creek displays the lowest social vulnerability, however, there are few citizens residing in this area, as it is an industrial sector, resulting in little to no SVI data (Figures 4 and A1). Altogether, the region of North Asheville has the lowest social vulnerability. Morningside/West Asheville Estates have low social vulnerability, making it an outlier to the wider adjacent communities (Figures 4 and A1).

4.1.3 Heat Vulnerability Analysis

The heat vulnerability map (Figure 5) combines the urban heat and social vulnerability indices, to display heat-vulnerable areas in Asheville, NC. The area with the highest heat vulnerability was the city center and surrounding downtown Asheville (Figures 5 and A1). The areas with the lowest heat vulnerability were generally located towards or adjacent to the CoA's periphery. One area inconsistent with this radial pattern was the census block group south of Shiloh and north of Arden, which had relatively high heat vulnerability, influenced by high urban heat and moderate social vulnerability (Figures 5 and A1). Overall, there was a pronounced pattern of decreasing heat vulnerability further away from downtown.

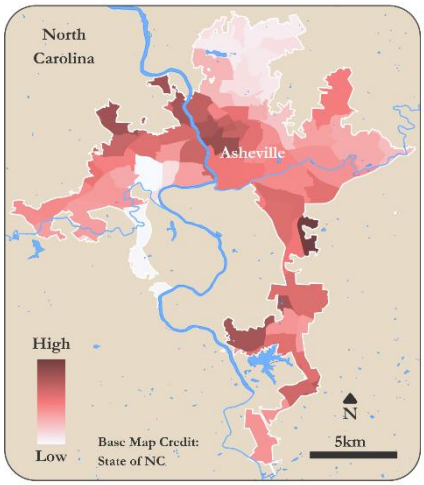

Figure 4. Social Vulnerability Map of Asheville, NC

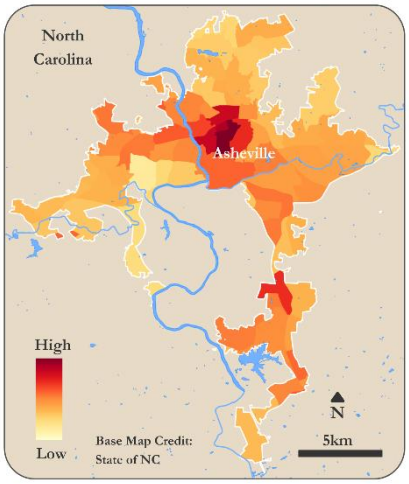

Figure 5. Heat Vulnerability Map of Asheville, NC

4.1.4 Cooling Capacity Analysis

The urban heat mitigation and adaptation map displays the present cooling capacity (the ability to mitigate or adapt to high urban heat) of census block groups (Figure 6). Canopy cover, evapotranspiration rates, and albedo all contribute to adaptation and mitigation capacity in this model. Broadly, North and East Asheville have the greatest cooling capacity (Figures 6 and. A1). The Oak Forest neighborhood in South Asheville stands out due to its relatively high capacity to mitigate and adapt to heat compared to surrounding census block groups (Figures 6 and. A1). West Asheville has a moderately high cooling capacity. The area with the lowest cooling capacity was downtown Asheville. (Figures 6 and. A1). This is followed by areas surrounding the downtown, such as the South Slope, the River Arts District, North Downtown, and those in the southern extent of the city, such as Arden and the airport area (Figures 6 and. A1). Generally, the areas in the CoA with dense canopy cover and less urban build-up or sprawl had higher cooling capacity.

The adaptive capacity map combines the output from the InVEST Urban Cooling Model (Figure 6) with the heat vulnerability index output (Figure 5). The downtown area (encompassing downtown, North downtown, and the South Slope) and Oak Forest in South Asheville had the highest heat vulnerability and the lowest cooling capacity, indicating that this area is the most in need of urban heat mitigation efforts (Figure 7 and A1). Factors contributing to the low cooling capacity and high heat vulnerability were a relative lack of trees and vegetation, high urban heat, and high social vulnerability. Alternatively, areas with high cooling capacity and low heat vulnerability, such as North Asheville (including Beaverdam and Grove Park/Sunset), East Asheville, and most of southern West Asheville, are not priority areas for cooling measures (Figure 7 and A1). Factors contributing to the high cooling capacity and low heat vulnerability were relatively more vegetation and canopy cover, lower urban heat, and lower social vulnerability.

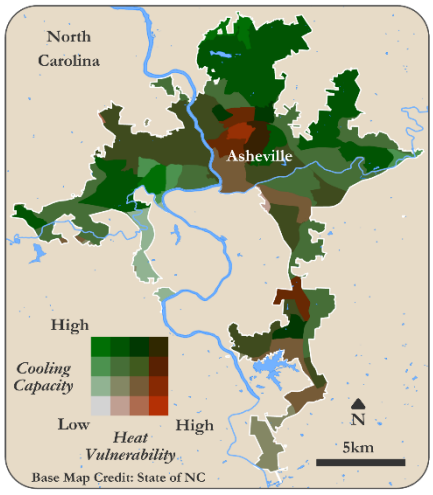

Figure 6. Urban Heat Mitigation and Adaption Map

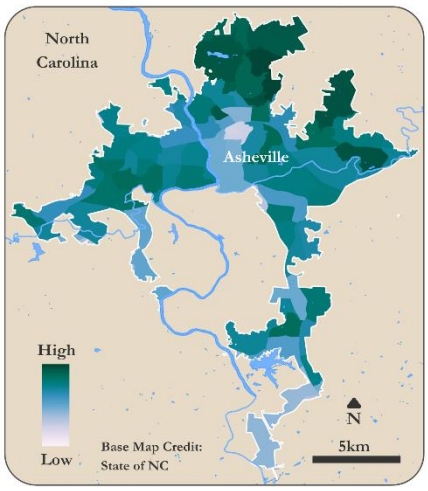

Figure 7. Cooling Capacity Map

4.2 Errors & Uncertainties

One limitation of the methodology of our study was the scale used for our analysis. Census block groups aggregate the data into larger spatial areas, obscuring variability within block groups. Depiction of the data at a more granular level, such as at the census block scale could highlight UHIs and other spatial patterns of heat vulnerability more accurately than block groups.

There were also limitations and possible points of uncertainty in our LST, albedo, and evapotranspiration methodologies. First, LST differs from ambient air temperature. LST is the temperature of the surface, while the air temperature is above the surface and what people typically feel. LST is generally hotter than the air temperature, making Asheville appear hotter on our maps than what people experience. Despite this, we used

LST as an indicator of urban heat because satellite remote sensors provide more spatial resolution than weather stations (Li et al., 2023).

Additionally, the relationship between albedo and LST is complex, creating a point of uncertainty in our study. In general, low albedo is correlated with increased LST, however, other environmental factors can modify how albedo is absorbed or reflected. Vegetation has relatively low albedo, absorbing more heat than reflective surfaces such as buildings, however, plants convert the absorbed energy into latent heat, which does not increase the environmental temperature. Furthermore, plants also reduce temperature through evapotranspiration and absorption of carbon dioxide. In contrast, while highly built-up areas in downtown Asheville have relatively high albedo, the proportion of absorbed insolation is instead converted to conventional heat, leading to pronounced increases in temperature (Nuruzzaman, 2015; Stache et al., 2022). We used mean evapotranspiration calculations, rather than median, as done with our other variables. In more extensive studies, we would create a tool to calculate the median value for consistency with the LST and albedo data. Finally, the evapotranspiration product we used did not have data available for 2023.

Our social vulnerability methodology had limitations. We used the CDC/ASTDR SVI because this index is the national standard for evaluating social vulnerability due to its large scope and data reliability. However, the demographic and socioeconomic variables measured in the SVI are not heat-specific (Center for Disease Control and Prevention, n.d.). It does not include specific contributing elements to heat vulnerability such as access to reliable home air-conditioning or air-conditioned spaces, home cooling energy burden, or specific health factors that make an individual more prone to heat-related health effects (Center for Disease Control and Prevention, n.d.). At the time of this study, there were no standardized, reliable heat vulnerability indices.

Our data processing method of data exclusion based on cloud cover limited our analysis. Depending on their height and structure, clouds can either cool or warm LST by reflecting isolation or trapping heat, impacting LST (Tselioudis, 2017). Therefore, our LST results may be slightly imprecise due to the exclusion of cloudy-day measurements. However, the margin of error is minimal since clouds can both warm and cool LST, preventing significant bias in one direction.

The time and aspect that the Landsat satellites pass over Asheville, NC affect the measurements recorded. The Landsat satellites pass over at roughly 11 am EST, so temperatures are not yet at the daily maximum as they are during the mid-afternoon (U.S. Geological Survey, 2020). Additionally, aspect can impact LST. In the morning when the satellite LST measurements are taken, the eastern side of the mountains is hotter than the western side, as this side was exposed to the sun for a longer duration.

Our calculations and analysis also had limitations. The min-max normalization we used to standardize our data does not process outliers well, which could have skewed the data. We did not conduct statistical analyses, which, if conducted, would have made our evaluation of the correlation between variables (e.g. our heat vulnerability analysis between hot spots and socially vulnerable areas) more robust. Furthermore, there were possible errors from our data processing. For instance, there were three census block groups with abnormally high albedo, possibly indicating errors that arose from the data processing, potentially from the cloud masking.

4.3 Feasibility & Partner Implementation

It was feasible to use NASA Earth observations to identify neighborhoods in the CoA most in need of heat mitigation strategies. Our project produced maps and data layers that will be helpful for our partners' decision-making processes forward. Our end products will add essential information to the CoA's preexisting Climate Justice Index and Climate Justice Map, providing the CoA with data for targeted urban heat intervention and climate resilience planning. If needed, our partners could further our methodology by rescaling the maps to a more granular block level to reveal more detail about UHI hot spots and by adding additional layers to the map package, such as heat-specific health data, and a CoA- specific LULC layer.

5. Conclusions

Our analysis revealed the spatial interaction between urban heat, heat vulnerability, and cooling capacity in Asheville, NC. Asheville's urban heat island effect is characterized by a radial pattern of decreasing urban heat from downtown to more rural areas, driven by the correlation between high LST and dense urban development with minimal vegetation and evapotranspiration. Socially vulnerable communities are disproportionately located in urban heat hotspots, indicating environmental injustices. Implementing cooling measures, such as urban greening and adding green or high albedo roofs in hotspots based on the urban landscape, can mitigate urban heat effects. For instance, green roofs could be considered in areas like downtown Asheville where additional tree planting is not possible, and the existing albedo is high. Our project emphasizes the need for targeted interventions to reduce heat impacts, address environmental injustices, and enhance urban climate resilience. These data will update Asheville's Climate Justice Map and inform the City of Asheville and Asheville GreenWorks' future heat mitigation strategies, including strategic tree planting, installation of cooling pavements, and green or white roofs.

6. Acknowledgements

We thank Tallis Monteiro, the NASA DEVELOP North Carolina NCEI Node Center Lead, for her leadership throughout this project. Thank you to our science advisors, Douglas Rao (NOAA National Centers for Environmental Information), Edward Macie (Asheville GreenWorks, CoA Urban Forestry Commission), and Molly Woloszyn (NOAA National Integrated Drought Information System) for their mentorship, guidance, and assistance. Chris Defiore, Eric Bradford, and Sara Millar from Asheville GreenWorks and Chris Clarke, Kiera Bulan, and Bridget Herring from the City of Asheville Sustainability Department deserve thanks for their partnership and collaboration. We would like to extend our appreciation to Kathryn Caruso (prior Center Lead for the NC – NCEI NASA DEVELOP Node) for developing the project, and Jared Rennie (NOAA National Centers for Environmental Information) and Kenton Ross (NASA Langley Research Center) for their guidance with data acquisition and processing. Representatives from NASA and the National Oceanic and Atmospheric Administration's National Center for Environmental Information deserve acknowledgement and thanks for their instruction and guidance.

Any opinions, findings, and conclusions or recommendations expressed in this material are those of the authors and do not necessarily reflect the views of the National Aeronautics and Space Administration.

This material is based upon work supported by NASA through contract 80LARC23FA024.

This material contains modified Copernicus Sentinel data (2021), processed by ESA.

7. Glossary

Albedo – the degree to which a surface absorbs or reflects insolation (incoming solar radiation).
Earth observations – Temporal and spatial information about Earth's physical, chemical, and biological systems, collected by satellites and sensors.
ECOSTRESS – ECOsystem Spaceborne Thermal Radiometer Experiment on Space Station is an Earth observation program recording evaporation and transpiration, evapotranspiration.
Evapotranspiration – the combined process of transpiration from vegetation, the process of evaporation from leaf pores, and soil evaporation.
Insolation – Incoming short-wave solar radiation to Earth's surface.
InVEST Urban Cooling Model – "calculates an index of heat mitigation based on shade, evapotranspiration, and albedo, as well as distance from cooling islands (e.g. parks)" (Stanford University, n.d.).
Landsat – NASA and USGS satellite program that uses electromagnetic sensors to record reflected insolation from Earth's surface, creating Earth observations.
Land surface temperature (LST) – the temperature of land surfaces, such as bare ground, vegetation, and unnatural human-made land covers – differs from air temperature.

Redlining – Redlining regarding housing practices refers to discrimination by denying services, such as the denial of loans or investments for residents of certain communities, based on the race or ethnicity of residents.
Remote sensing – the process of using electromagnetic sensors to actively or passively detect and record energy that is reflected or emitted from Earth's surface.
Urban heat island (UHI) effect – the phenomenon whereby urbanized areas or cities experience higher temperatures than adjacent rural areas.

8. References

Agrawal, A., Kalra, A., Machuca, V., Sik Cho, M., & Farid, Z. (2022). UHEAT Urban Development: Increasing Capabilities and Updating the Urban Heat Exposure Assessment for Tempe (UHEAT) Tool [Unpublished tool]. NASA DEVELOP National Program, Pop-up Project.

AppEEARS Team. (2024). *Application for Extracting and Exploring Analysis Ready Samples (AppEEARS).* (V3.56) [Data set]. NASA EOSDIS Land Processes Distributed Active Archive Center (LP DAAC). USGS/Earth Resources Observation and Science (EROS) Center, Sioux Falls, South Dakota, USA. Retrieved June 27, 2024, from https://appeears.earthdatacloud.nasa.gov/.

Asheville GreenWorks. (2022). *About us — Asheville GreenWorks*. Retrieved June 25, 2024, from https://www.ashevillegreenworks.org/about.

Bao, J., Li, X., & Yu, C. (2015). The Construction and Validation of the Heat Vulnerability Index, a Review. *International Journal of Environmental Research and Public Health*, 12(7), 7220–7234. https://doi.org/10.3390/ijerph120707220.

Center for Disease Control and Prevention. (n.d.). *CDC ATSDR Social Vulnerability Index*. Retrieved June 27, 2024, from https://www.atsdr.cdc.gov/placeandhealth/svi/index.html.

City of Asheville. (2018). Canopy Cover [Data Set]. https://data-avl.opendata.arcgis.com/maps/eb42769291b346c7ba83992adaa9ecfd/about

Environmental Protection Agency. (n.d.). *Heat Island effect*. US EPA. Retrieved June 14, 2024, from https://www.epa.gov/heatislands

Gray, D., Kalra, A., & Kennedy, A. (2019). Asheville Urban Development: Using NASA Earth Observations to Quantify the Impact of Urban Tree Canopy Cover on Urban Heat and Identify Community Vulnerability in Asheville, North Carolina [Unpublished manuscript]. NASA DEVELOP National Program, NCEI.

Hook, S. & Fisher, J. (2019). *ECOSTRESS Evapotranspiration PT-JPL Daily L3 Global 70 m* (V001) [Data set]. NASA EOSDIS Land Processes Distributed Active Archive Center. Retrieved August 01, 2024, from https://doi.org/10.5067/ECOSTRESS/ECO3ETPTJPL.001

Knight, T., Price, S., Hookway, A., King, S., & Richter, R. (2021). How effective is 'greening' of urban areas in reducing human exposure to ground-level ozone concentrations, UV exposure and the 'urban heat island effect'? An updated systematic review. Environmental Evidence, 10(12). https://environmentalevidencejournal.biomedcentral.com/articles/10.1186/s13750-021-00226-y

Li, Z., Wu, H., Duan, S., Zhao, W., Ren, H., Liu, X., Leng, P., Tang, R., Ye, X., Zhu, J., Sun, Y., Si, M., Liu, M., Li, J., Zhang, X., Shang, G., Tang, B., Yan, G., & Zhou, C. (2023). Satellite Remote sensing of global land surface temperature: definition, methods, products, and applications. *Reviews of Geophysics*, *61*(1), e2022RG000777. https://doi.org/10.1029/2022rg000777.

Mitchell, B. C. & Chakraborty, J. (2015). Landscapes of thermal inequity: Disproportionate exposure to urban heat in the three largest US cities. *Environmental Research Letters*, *10*(11), 115005. https://doi.org/10.1088/1748-9326/10/11/115005.

Moss, J. L., Doick, K. J., Smith, S., & Shahrestani, M. (2019). Influence of evaporative cooling by urban forests on cooling demand in cities. *Urban Forestry & Urban Greening*, 37, 65-73. https://doi.org/10.1016/j.ufug.2018.07.023.

Nuruzzaman, M.D. (2015). Urban Heat Island: Causes, Effects and Mitigation Measures - A Review. I*nternational Journal of Environmental Monitoring and Analysis*, 3(2), 67–73. https://doi.org/10.11648/j.ijema.20150302.15

Phelan, P. E., Kaloush, K., Miner, M., Golden, J., Phelan, B., Silva, H., & Taylor, R. A. (2015). Urban Heat Island: mechanisms, implications, and possible remedies. *Annual Review of Environment and Resources*, *40*(1), 285–307. https://doi.org/10.1146/annurev-environ-102014-021155.

Qiu, G., Li, H., Zhang, Q., Chen, W., Liang, X., & Li, X. (2013). Effects of Evapotranspiration on Mitigation of Urban Temperature by Vegetation and Urban Agriculture. *Journal of Integrative Agricultur*e, 12(8), 1307–1315. https://doi.org/10.1016/s2095-3119(13)60543-2.

Reid, C. E., O'Neill, M. S., Gronlund, C. J., Brines, S. J., Brown, D. G., Diez-Roux, A. V., & Schwartz, J. (2009). Mapping community determinants of heat vulnerability. *Environmental Health Perspectives*, 117(11), 1730–1736. https://doi.org/10.1289/ehp.0900683.

Shahmohamadi, P., Che-Ani, A., Etessam, I., Maulud, K., & Tawil, N. (2011). Healthy environment: The need to mitigate urban heat island effects on human health. *Procedia Engineering*, 20, 61–70. https://doi.org/10.1016/j.proeng.2011.11.139.

Stache, E., Schilperoort, B., Ottelé, M., & Jonkers, H. (2022). Comparative analysis in thermal behaviour of common urban building materials and vegetation and consequences for urban heat island effect. *Building and Environment*, 213(1), 108489. https://doi.org/10.1016/j.buildenv.2021.108489.

Stanford University. (n.d.). *Urban cooling*. Stanford University Natural Capital Project. Retrieved June 26, 2024, from https://naturalcapitalproject.stanford.edu/invest/urban-cooling.

Swope, C. B., Hernández, D., & Cushing, L. J. (2022). The Relationship of Historical Redlining with Present-Day Neighborhood Environmental and Health Outcomes: A Scoping Review and Conceptual model. *Journal of Urban Health*, *99*(6), 959–983. https://doi.org/10.1007/s11524-022-00665-z.

The City of Asheville. (2019, October 29). *Asheville Urban Tree Canopy Study looks at canopy loss and opportunities to preserve it*. https://www.ashevillenc.gov/news/asheville-urban-tree-canopy-study-looks-at-canopy-loss-and-opportunities-to-preserve-it/.

The City of Asheville. (2020). Resolution 20-25 Climate Emergency Declaration. In *City of Asheville Sustainability Department*. Retrieved June 25, 2024, from https://www.ashevillenc.gov/department/sustainability/climate-initiatives/.

The City of Asheville. (n.d.). *Climate Justice initiative*. Retrieved June 25, 2024, from https://www.ashevillenc.gov/department/sustainability/climate-initiatives/climate-justice-initiative/.

The City of Asheville. (n.d.-a). *City of Asheville Climate Justice Index*. Retrieved June 25, 2024, from https://avl.maps.arcgis.com/apps/instant/lookup/index.html?appid=10e2c4ae45614b92ad4efaa61342b249

The City of Asheville Urban Forestry Commission. (2023). 2022 Urban Forestry Commission Annual Report. In *The City of Asheville*. The City of Asheville. Retrieved June 25, 2024, from https://docs.google.com/document/d/1g2vceKGb5Uqr-SgCHtsGR20gyml3vC-k/edit

Tong, S., Prior, J., McGregor, G., Shi, X., & Kinney, P. (2021). Urban heat: an increasing threat to global health. *Building Healthy Communities*, PMC8543181. https://doi.org/10.1136/bmj.n2467.

Tselioudis, G. (2017). *Cloud climatology*. International Satellite Cloud Climatology Project. Retrieved July 18, 2024, from https://isccp.giss.nasa.gov/role.html.

U.S. Census Bureau. (n.d.). *U.S. Census Bureau QuickFacts: Asheville city, North Carolina*. Retrieved June 18, 2024, from https://www.census.gov/quickfacts/fact/table/ashevillecitynorthcarolina

U.S. Geological Survey (2020). *Landsat 8-9 OLI (Operational Land Imager) and TIRS (Thermal Infrared Sensor) Collection 2 Level- 2 Science Products* [Data set]. U.S. Geological Survey. Retrieved July 23, 2024, from https://doi.org/10.5066/P9OGBGM6.

U.S. Geological Survey. (2023). *LandsatLook*. Retrieved July 23, 2024, from https://landsatlook.usgs.gov/explore?date=2021-10-31%7C2023-07-16.

Weber, S., Sadoff, N., Zell, E., & de Sherbinin, A. (2015). Policy-relevant indicators for mapping the vulnerability of urban populations to extreme events: a case study of Philadelphia. *Applied Geography*, *63*, 231-243. https://doi.org/10.1016/j.apgeog.2015.07.006.

Yale University. (n.d.). *How to convert Landsat DNs to Albedo*. Center for Earth Observations. Retrieved July 18, 2024, from https://yceo.yale.edu/how-convert-landsat-dns-albedo

Zanaga, D., Van De Kerchove, R., Daems, D., De Keersmaecker, W., Brockmann, C., Kirches, G., Wevers, J., Cartus, O., Santoro, M., Fritz, S., Lesiv, M., Herold, M., Tsendbazar, N.E., Xu, P., Ramoino, F., & Arino, O. (2021) *ESA WorldCover 10m 2021* (v200) [Data Set]. European Space Agency. Retrieved August 07, 2024, from https://doi.org/10.5281/zenodo.7254221.

9. Appendices

Appendix A: *Map of Asheville, NC Districts and Neighborhoods*

Figure A1. Map of Asheville, NC districts and neighborhoods referenced within this report